

# Crystal Structures of the Oxidized and Reduced Forms of UDP-galactose 4-Epimerase Isolated from *Escherichia coli*<sup>†,‡</sup>

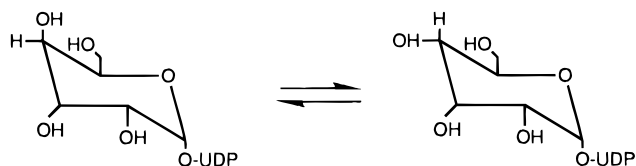
James B. Thoden, Perry A. Frey, and Hazel M. Holden\*

*Institute for Enzyme Research, Graduate School, and Department of Biochemistry, University of Wisconsin, Madison, Wisconsin 53705*

*Received November 14, 1995; Revised Manuscript Received December 11, 1995*<sup>§</sup>

**ABSTRACT:** UDP-galactose 4-epimerase catalyzes the conversion of UDP-galactose to UDP-glucose through a mechanism involving the transient reduction of NAD<sup>+</sup>. Here we describe the X-ray structures for epimerase complexed with NADH/UDP and NAD<sup>+</sup>/UDP, refined to 1.8 and 2.0 Å, respectively. The α-carbon positions for the two forms of the enzyme are superimposed with a root-mean-square deviation of 0.36 Å. Overall, the models for the reduced and oxidized proteins are very similar except for the positions of several side chains including Phe 178 and Phe 218. The most striking difference between the oxidized and reduced enzymes is the conformation of the nicotinamide ring of the dinucleotide. In the reduced protein, the nicotinamide ring adopts the *anti* conformation while in the oxidized enzyme the *syn* conformation is observed. There are also significant structural differences in UDP binding between the oxidized and reduced forms of the protein which most likely explain the observation that uridine nucleotides bind more tightly to epimerase/NADH than to epimerase/NAD<sup>+</sup>. Both van der Waals and electrostatic interactions between epimerase and NAD<sup>+</sup> are extensive with 35 contacts below 3.2 Å as would be expected for an enzyme that binds the dinucleotide irreversibly. This is in sharp contrast to the patterns typically observed for the NAD<sup>+</sup>-dependent dehydrogenases which bind nucleotides in a reversible fashion. While it has been postulated that the active site of epimerase must contain a base, the only potential candidates within approximately 5 Å of both the NAD<sup>+</sup> and the UDP are Asp 31, Asp 58, and Asp 295. These amino acid residues, however, are intimately involved in nucleotide binding and most likely do not play a role in the actual catalytic mechanism. Thus it may be speculated that an amino acid residue, other than glutamate, aspartate, or histidine, may be functioning as the active site base.

The metabolic steps by which galactose, one of the products of lactose hydrolysis, is converted into glucose 1-phosphate are known as the Leloir pathway. UDP-galactose 4-epimerase, the focus of this paper and hereafter referred to as epimerase, catalyzes the third reaction in this pathway where it interconverts UDP-galactose and UDP-glucose.



As isolated from *Escherichia coli*, the enzyme is a homodimer with each subunit containing 338 amino acid residues and one nicotinamide adenine dinucleotide (NAD<sup>+</sup>) (Wilson & Hogness, 1969; Lemaire & Müller-Hill, 1986; Bauer *et al.*, 1992). The proposed catalytic mechanism for epimerase that is in best agreement with the present biochemical and biophysical data involves the transient reduction of the NAD<sup>+</sup> cofactor (Frey, 1987). According to the current hypothesis, substrate binding to epimerase leads to a conformational change in the enzyme which has the

effect of activating the cofactor toward reduction (Bertland & Kalckar, 1968; Kang *et al.*, 1975). Abstraction of the C-4 hydroxyl hydrogen of the sugar by a putative active site base and transfer of a hydride from C-4 to NAD<sup>+</sup> leads to the formation of a 4-ketose intermediate. A unique feature of the epimerase reaction is the promotion of nonstereospecific hydride transfer between NAD<sup>+</sup> and a chiral substrate. This is in sharp contrast to the NAD<sup>+</sup>-dependent dehydrogenases that undergo stereospecific hydride transfer (Walsh, 1979). The nonstereospecificity displayed by epimerase is thought to occur through the free rotation of the 4-ketose intermediate about the phosphoryl–oxygen bond connecting the UDP and sugar moieties, thereby leading to a change in the spatial relationship between the intermediate and the NADH cofactor (Kang *et al.*, 1975). Such putative rotation of the intermediate allows for the return of the hydride from the B-side of NADH to the 4-ketose moiety. The product is formed by the reprotonation of the hexose. This reaction is readily reversible such that UDP-glucose is converted into UDP-galactose under certain physiological conditions.

We initiated an X-ray crystallographic analysis of epimerase as purified from *E. coli* in order to address the various structural issues associated with the enzyme, including the nonstereospecificity of hydride transfer, the ability of various reducing sugars to inactivate the enzyme in the presence of uridine nucleotides, and the tight binding of the nicotinamide adenine dinucleotide cofactor to the protein. The initial three-dimensional model for the enzyme was obtained from crystals of the protein complexed with the substrate analog UDP-phenol (Bauer *et al.*, 1992). A ribbon representation of one of the subunits is shown in Figure 1. As can be seen,

<sup>†</sup> This research was supported in part by grants from the NIH (DK47814 to H.M.H., GM15950 to J.B.T., and GM30480 to P.A.F.).

<sup>‡</sup> Coordinates for the reduced and oxidized forms of epimerase have been deposited in the Brookhaven Protein Data Bank under the identification codes 1NAH and 1NIA, respectively.

\* To whom correspondence should be addressed.

<sup>§</sup> Abstract published in *Advance ACS Abstracts*, February 1, 1996.

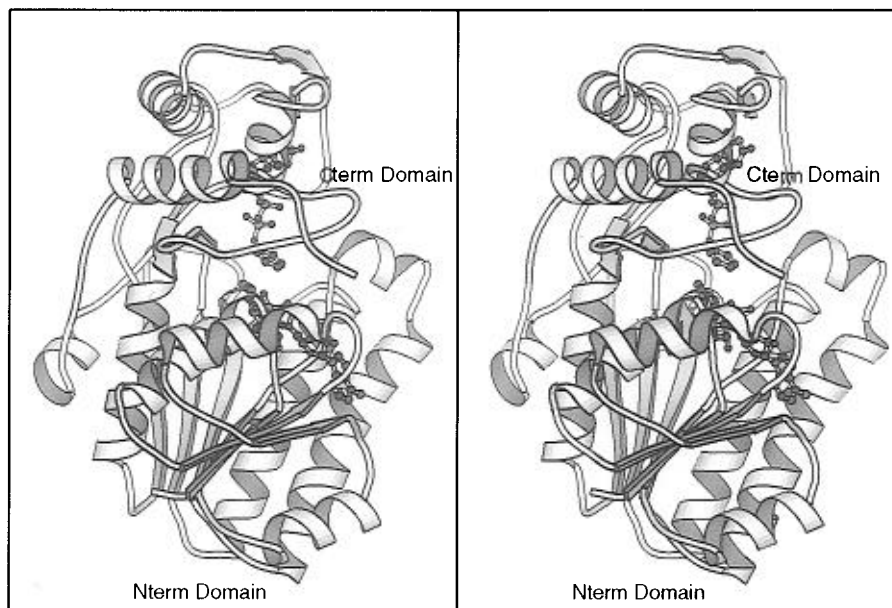


FIGURE 1: Ribbon representation of one subunit of epimerase with bound  $\text{NAD}^+$  and UDP-phenol. This figure was prepared with the X-ray coordinates determined by Bauer *et al.* (1992) and the software package MOLSCRIPT (Kraulis, 1991). The  $\text{NAD}^+$  and UDP-phenol are depicted in ball-and-stick representations. The aromatic ring of the UDP-phenol is located near the middle of the subunit.

the polypeptide chain folds into two distinct structural motifs as typically observed in the  $\text{NAD}^+$ -dependent dehydrogenases with the substrate analog binding in the cleft formed by the two domains. The larger N-terminal domain of the subunit is composed of approximately 180 amino acid residues and adopts a modified dinucleotide binding motif with seven strands of parallel  $\beta$ -pleated sheet flanked on either side by  $\alpha$ -helices. The C-terminal domain contains three strands of  $\beta$ -pleated sheet, two major  $\alpha$ -helices, and one helical turn. In addition to allowing for a three-dimensional structure of the enzyme to be modeled, this X-ray crystallographic investigation proved that the protein binds two  $\text{NAD}^+$  molecules per dimer rather than one as originally believed (Wilson & Hogness, 1964). Due to the limited resolution of 2.5 Å, however, details concerning the active site and the solvent structure were not addressed. Furthermore, it was suggested that the presence of an aromatic group in the substrate analog perturbed the conformation of the  $\text{NAD}^+$  cofactor. Indeed, the nicotinamide ring adopted the *anti* rather than the *syn* conformation as would be expected for a B-side-specific enzyme.

Here we describe the three-dimensional structures of both the oxidized and reduced forms of epimerase crystallized in the presence of UDP and solved and refined to 2.0 and 1.8 Å, respectively. These studies have allowed for a more complete description of the secondary structure, the solvent structure, and the hydrogen-bonding patterns exhibited between the protein and the nucleotides. In addition, these investigations have demonstrated that the conformation of the nicotinamide ring, in relationship to the ribose, is apparently dependent upon the oxidation state of the cofactor.

## MATERIALS AND METHODS

**Purification and Crystallization Procedures.** Recombinant UDP-galactose 4-epimerase was expressed in an *E. coli* overproducing strain BL21(DE3), pLysS, carrying the expression plasmid pT7E2, as previously described (Swanson & Frey, 1993). Purification of the enzyme essentially

followed the method of Bauer *et al.* (1991) with the exception of the replacement of a Q-Sepharose fast-flow column for a DEAE-Sephadex A-50 column in the final step. The purified enzyme was stored at 30 mg/mL in 10 mM potassium phosphate (pH 7.0) at  $-130^\circ\text{C}$ . Enzymatic activity was monitored with the coupled assay described by Wilson and Hogness (1964). It is known from previous investigations that purified epimerase contains small amounts of NADH (Wong *et al.*, 1978). For the crystallization experiments described here the specific activity of the enzyme was 10 500 units/mg. The highest value observed for purified epimerase has been 13 000 units/mg (Vanhook & Frey, 1994).

The hanging drop method of vapor diffusion was employed for crystallization of both the oxidized and reduced forms of the enzyme. All crystallization experiments were conducted at  $4^\circ\text{C}$ . For the epimerase/ $\text{NAD}^+$ /UDP complex, the enzyme was first concentrated to approximately 60 mg/mL and incubated for 2 h at room temperature with 5 mM UDP. Subsequently, 10  $\mu\text{L}$  of the protein solution was mixed on silanized glass coverslips with 10  $\mu\text{L}$  of a solution containing 15% poly(ethylene glycol) 8000 (PEG), 500 mM NaCl, and 50 mM HEPES (pH 8.0). These droplets were equilibrated against 15% PEG. Crystals generally appeared within 24 h and achieved maximum dimensions of 0.8 mm  $\times$  0.8 mm  $\times$  0.8 mm within 1 week. They belonged to the space group  $P3_221$  with unit cell dimensions of  $a = b = 83.5$  Å,  $c = 108.2$  Å, and one subunit per asymmetric unit.

The reduced form of the epimerase was obtained by first incubating the enzyme, at 30 mg/mL, for 2 h at room temperature with 5 mM UDP and then adding, over a 4 h period, three aliquots of a 1.5 M dimethylamine–borane complex solution to yield a final concentration of 200 mM for the reductant. This mixture was allowed to incubate overnight at  $4^\circ\text{C}$  and was then dialyzed against 10 mM potassium phosphate (pH 8.0) for 24 h. The protein was concentrated to 60 mg/mL and incubated for another 2 h with 5 mM UDP at  $4^\circ\text{C}$ . Crystallization experiments were conducted in a similar manner as described above except

Table 1: Intensity Statistics for the Reduced Form of Epimerase

	resolution range (Å)							
	overall	30.00–4.00	3.11	2.63	2.32	2.10	1.93	1.80
no. of measurements	72653	10674	8230	10402	10728	10968	11050	10601
no. of independent reflections	39891	3848	4208	5177	5872	6526	7044	7216
completeness of data (%)	97	98	98	99	98	98	96	94
av intensity	165	391	329	135	76	54	31	17
av $\sigma$	6.3	10.5	8.6	4.2	2.7	2.6	2.1	1.7
<i>R</i> factor <sup>a</sup> (%)	2.1	1.5	1.7	2.2	2.7	3.5	5.1	7.6

<sup>a</sup> *R* factor =  $(\sum |I - \bar{I}| / \sum I) \times 100$ .

Table 2: Intensity Statistics for the Oxidized Form of Epimerase

	resolution range (Å)							
	overall	30.00–4.00	3.11	2.63	2.32	2.10	1.93	1.80
no. of measurements	63946	9554	7403	9098	9252	9549	9874	9216
no. of independent reflections	39504	3769	4148	5102	5860	6475	7028	7122
completeness of data (%)	96	96	97	98	98	98	95	93
av intensity	220	521	392	146	75	46	22	12
av $\sigma$	15.5	26.7	16.8	7.2	5.1	4.5	3.7	3.3
<i>R</i> factor <sup>a</sup> (%)	3.4	2.4	2.7	3.6	5.0	7.5	12.9	22.5

<sup>a</sup> *R* factor =  $(\sum |I - \bar{I}| / \sum I) \times 100$ .

the precipitant was 20% PEG 8000, 500 mM NaCl, and 50 mM CHES (pH 9.0). Again crystals appeared within 24 h and achieved maximum dimensions of 1 mm  $\times$  1 mm  $\times$  1 mm. They also belonged to the space group *P*<sub>3</sub>2<sub>1</sub> with unit cell dimensions of *a* = *b* = 83.5 Å, *c* = 108.4 Å, and one subunit per asymmetric unit.

**X-ray Data Collection and Processing.** Prior to X-ray data collection, crystals of the epimerase/NAD<sup>+</sup>/UDP complex were transferred to a synthetic mother liquor containing 15% PEG 8000, 500 mM NaCl, 5 mM UDP, and 50 mM HEPPS (pH 8.0) and allowed to soak for 1 h after which time they were serially transferred, in four steps over 10 min, to a cryoprotectant solution containing 20% PEG 8000, 750 mM NaCl, 50 mM HEPPS (pH 8.0), and 20% ethylene glycol. Crystals were suspended in a thin film of the cryoprotectant mixture using a loop composed of fine surgical thread and flash-cooled to  $-150^\circ\text{C}$  in a nitrogen stream. The identical procedure was employed for the epimerase/NADH/UDP complex except that the synthetic mother liquor contained 20% PEG, 500 mM NaCl, and 50 mM CHES (pH 9.0) and the cryoprotectant solution was composed of 25% PEG, 750 mM NaCl, and 20% ethylene glycol.

X-ray data for both crystal complexes were collected at  $-150^\circ\text{C}$  with a Siemens HI-STAR dual area detector system equipped with double-focusing mirrors. The X-ray source was Cu K $\alpha$  radiation from a Rigaku RU200 rotating anode generator operated at 50 kV and 90 mA and equipped with a 300  $\mu\text{m}$  focal cup. Only one crystal was required per X-ray data set.

The X-ray data were processed according to the procedure of Kabsch (1988a,b) and internally scaled according to the algorithm of Fox and Holmes (1966) as implemented by Dr. Phil Evans. The X-ray data sets were 96% and 97% complete to 2.0-Å and 1.8-Å resolution for the oxidized and reduced crystal forms, respectively. Relevant X-ray data collection statistics may be found in Tables 1 and 2.

**Computational Methods.** The structures of both the oxidized and reduced forms of the enzyme were solved by the technique of molecular replacement with the software package AMORE (Rossmann, 1972; Navaza, 1987). The

Table 3: Least Squares Refinement Statistics for the Reduced Enzyme

resolution limits (Å)	30.0–1.8
<i>R</i> factor <sup>a</sup> (%)	16.5
no. of reflections used	39891
no. of protein atoms	2694
no. of solvent atoms	505
weighted root-mean-square deviations from ideality	
bond length (Å)	0.015
bond angle (deg)	2.2
planarity (trigonal) (Å)	0.008
planarity (other planes) (Å)	0.013
torsional angle <sup>b</sup> (deg)	14.9

<sup>a</sup> *R* factor =  $\sum |F_o - F_c| / \sum |F_o|$ , where *F*<sub>o</sub> is the observed structure factor amplitude and *F*<sub>c</sub> is the calculated structure factor amplitude.

<sup>b</sup> The torsional angles were not restrained during the refinement.

structure of the enzyme complexed with UDP-phenol served as the search model. Both the rotational and translational searches were conducted with X-ray data from 8 to 4 Å. The following solutions were obtained for the oxidized and reduced forms of the protein, respectively:  $\alpha = 0.77^\circ$ ,  $\beta = 54.7^\circ$ ,  $\gamma = 89.4^\circ$ , *a* = 0.3034, *b* = 0.0074, and *c* = 0.3519 and  $\alpha = 0.85^\circ$ ,  $\beta = 46.1^\circ$ ,  $\gamma = 88.6^\circ$ , *a* = 0.3047, *b* = 0.0134, and *c* = 0.3514. Following rigid body refinement with X-ray data between 20 to 4 Å, the *R* factors for the oxidized and reduced proteins were reduced to 35.6% and 30.2%, respectively.

The three-dimensional models were refined by multiple cycles of manual model building with the program FRODO and least squares refinement with the software package TNT (Jones, 1985; Tronrud *et al.*, 1987). Ideal stereochemistries for the NAD<sup>+</sup> and UDP moieties were based on the small molecule structural determinations of Reddy *et al.* (1981) and Viswamitra *et al.* (1979), respectively. Restraints imposed on the nicotinamide ring of the reduced cofactor during least squares refinement were based on the results of Glasfeld *et al.* (1988). Relevant refinement statistics may be found in Tables 3 and 4.

**Quality of the X-ray Models.** The quality of the X-ray data to 1.8-Å resolution collected from the crystal of the

Table 4: Least Squares Refinement Statistics for the Oxidized Enzyme

resolution limits (Å)	30.0–2.0
<i>R</i> factor <sup>a</sup> (%)	19.3
no. of reflections used	29318
no. of protein atoms	2712
no. of solvent atoms	372
weighted root-mean-square deviations from ideality	
bond length (Å)	0.013
bond angle (deg)	2.2
planarity (trigonal) (Å)	0.007
planarity (other planes) (Å)	0.012
torsional angle <sup>b</sup> (deg)	15.6

<sup>a</sup> *R* factor =  $\sum |F_o - F_c| / \sum |F_o|$ , where *F<sub>o</sub>* is the observed structure factor amplitude and *F<sub>c</sub>* is the calculated structure factor amplitude.

<sup>b</sup> The torsional angles were not restrained during the refinement.

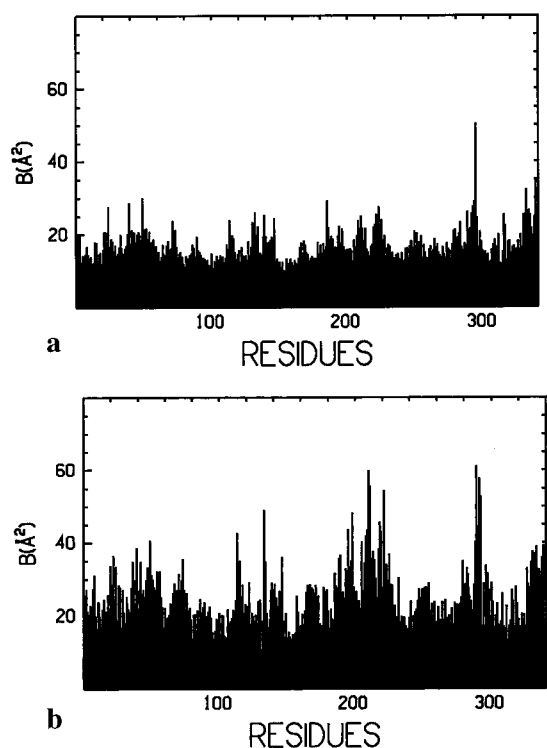


FIGURE 2: Mean main-chain temperature factor plots versus amino acid residue number. Shown are (a) the mean *B* values for the model of the reduced epimerase and (b) the mean *B* values for the oxidized protein.

reduced protein can be seen in Table 1. Even in the highest resolution bin, the *R*<sub>merge</sub> was only 7.6%. As a consequence the model was easily refined by least squares analysis to an *R* factor of 16.5% for all measured X-ray data. A plot of the mean main-chain temperature factors versus amino acid residue number is shown in Figure 2a. The average *B* value for the polypeptide chain backbone atoms was 16.8 Å<sup>2</sup>. There were no breaks in the electron density for the backbone, and almost all of the side chain groups were well-ordered except for the following residues: His 70, Glu 95, Gln 146, Lys 165, Lys 278, Lys 282, and Glu 293. A Ramachandran plot for all non-glycyl main-chain dihedral angles is displayed in Figure 3a. The only significant outlier was Phe 178 with  $\phi = -101^\circ$  and  $\psi = -104^\circ$ . This residue is located near the carboxamide group of the reduced cofactor.

Crystals of the oxidized enzyme do not diffract nearly as well to 1.8-Å resolution as can be seen from Table 2. In the highest resolution bin, the *R*<sub>merge</sub> was 22.5%. Conse-

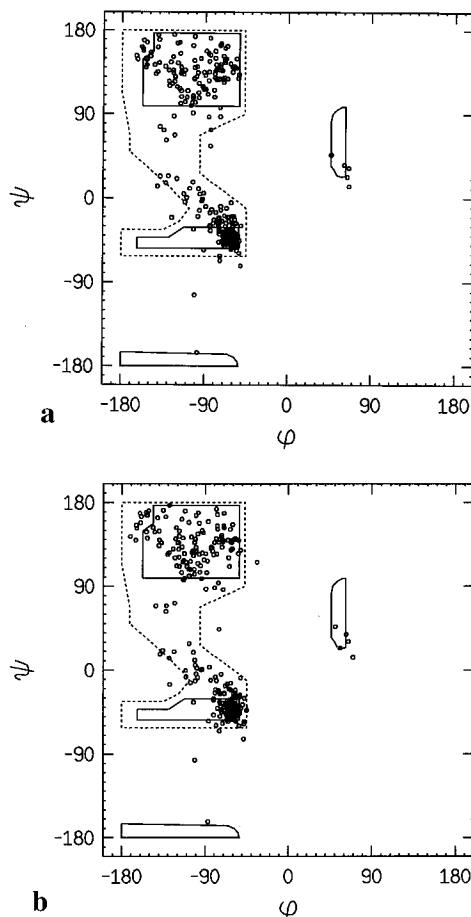


FIGURE 3: Ramachandran plots of all non-glycyl main-chain dihedral angles. Shown are the  $\phi, \psi$  angles for (a) the reduced and (b) the oxidized forms of epimerase. Fully allowed  $\phi, \psi$  values are enclosed by solid lines; those partially allowed are enclosed by dashed lines.

quently, the least squares refinement of the model for the oxidized protein was truncated to 2.0-Å resolution, and the *R* factor for all measured X-ray data was 19.3%. A plot of the mean main-chain temperature factors versus amino acid residue number is shown in Figure 2b. The average *B* value for the polypeptide chain backbone atoms was 26.0 Å<sup>2</sup>. Those regions in the main-chain backbone of the oxidized protein that demonstrated significantly higher *B* values were delineated by Asp 130 to Lys 133, Gln 194 to Asn 220, and Ala 289 to Leu 296. Note that the specific activity of the protein employed in this investigation suggests that a small portion of the protein in the crystalline lattice is in the reduced form. Whether these higher *B* values are a function of this mixed population or are an inherent property of the oxidized enzyme is not clear. Those side chains that were not well-ordered in the electron density map are as follows: Leu 47, Lys 92, Glu 95, Lys 117, Phe 140, Gln 146, Asn 198, Arg 211, and Lys 282. A Ramachandran plot for the model of the NAD<sup>+</sup>/UDP/epimerase complex is displayed in Figure 3b. As in the reduced enzyme, the only significant outlier was Phe 178 ( $\phi = -101^\circ$ ,  $\psi = -97^\circ$ ).

## RESULTS AND DISCUSSION

*Description of the Epimerase/UDP/NADH Complex.* An  $\alpha$ -carbon trace of one subunit of the epimerase/UDP/NADH complex is displayed in Figure 4. A list of the secondary structural elements may be found in Table 5. Nearly 79%

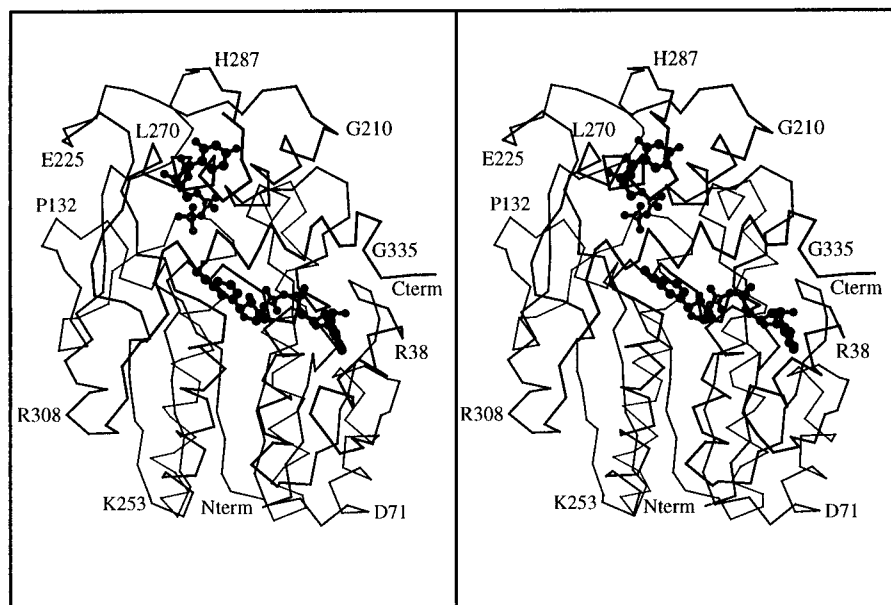


FIGURE 4:  $\alpha$ -Carbon trace of one subunit of the epimerase/UDP/NADH complex. Both nucleotides are displayed in ball-and-stick representations. Various amino acid residues are labeled to aid the viewer in following the course of the polypeptide chain.

Table 5: List of Secondary Structural Elements for the Epimerase/NADH/UDP Complex

residue no.	type of element	identifier	residue no.	type of element	identifier
Met 1–Leu 4	$\beta$ -sheet	B1	Pro 148–Ala 166	$\alpha$ -helix	A6
Val 5–Gly 8	$\sim$ type II turn		Gln 167–Trp 170	$\sim$ type I turn	
Gly 7–Gly 10	type I turn		Ser 171–Val 181	$\beta$ -sheet	B6
Tyr 11–Leu 20	$\alpha$ -helix	A1	His 184–Gly 187	type III turn	
Leu 21–Gly 24	type I turn		Leu 200–Gln 206	$\alpha$ -helix	A7
His 25–Asp 31	$\beta$ -sheet	B2	Val 207–Gly 210	type I turn	
Leu 33–Ser 36	$\sim$ type I turn		Ser 214–Phe 218	$\beta$ -sheet	B7
Arg 38–Glu 45	$\alpha$ -helix	A2	Thr 224–Gly 227	type I turn	
Arg 46–Gly 49	type I turn		Thr 228–His 235	$\beta$ -sheet	B8
Lys 50–Glu 56	$\beta$ -sheet	B3	Val 236–Lys 249	$\alpha$ -helix	A8
Asp 58–Asn 61	type III turn		Leu 250–Lys 253	$\sim$ type II turn	
Glu 62–Leu 69	$\alpha$ -helix	A3	Gly 255–Gly 262	$\beta$ -sheet	B9
His 70–Ala 73	type I turn		Val 265–Ser 268	$\beta$ -sheet	B10
Thr 76–His 79	$\beta$ -sheet	B4	Val 269–Ser 277	$\alpha$ -helix	A8
Val 86–Gln 91	$\alpha$ -helix	A4	Lys 278–Gly 281	type I turn	
Pro 93–Met 111	$\alpha$ -helix	A5	Asn 285–Pro 290	$\beta$ -sheet	B11
Arg 112–Asn 115	type I turn		Arg 292–Asp 295	type II turn	
Asn 118–Ser 123	$\beta$ -sheet	B5	Ala 298–Asp 302	$\beta$ -sheet	B12
Ser 124–Val 127	type III turn		Ser 304–Glu 309	$\alpha$ -helix	A9
Ala 125–Tyr 128	type III turn		Leu 318–Arg 331	$\alpha$ -helix	A10
Thr 126–Gly 129	type I turn		His 332–Gly 335	type I turn	
Val 137–Phe 140	type I turn				

of the amino acids lie within well-defined secondary structural elements including 12 strands of  $\beta$ -pleated sheet, 11  $\alpha$ -helices, 13 type I turns, 3 type II turns, and 4 type III turns. There is one *cis*-proline in the epimerase structure, namely Pro 135, which is located between two type I turns delineated by Thr 126 to Gly 129 and Val 137 to Phe 140. Of the 492 water molecules positioned into the electron density map, 192 have temperature factors below  $30 \text{ \AA}^2$ . In addition to these water molecules, there are two sodium ions, an ethylene glycol moiety, and one di(ethylene glycol) molecule included in the model. The di(ethylene glycol) surrounds the  $\epsilon$ -nitrogen of Lys 253 while the ethylene glycol is situated in the active site and lies within  $2.9 \text{ \AA}$  of the backbone amide nitrogen of Asp 192,  $2.7 \text{ \AA}$  of a water molecule, and  $2.4 \text{ \AA}$  of a phosphoryl oxygen of the NADH. The presence of an ethylene glycol molecule in the electron density map is not surprising in light of the fact that the cryoprotectant solution contained 20% ethylene glycol and

the active site of epimerase is very solvent accessible. Both sodium ions are located at the surface of the protein and are coordinated by oxygen-containing ligands in an octahedral arrangement. In each case, five of the six ligands are water molecules whereas the sixth ligand is either the carbonyl oxygen of Gln 334 or  $O^{\epsilon 1}$  of Gln 91. These sodiums were originally modeled as waters, but their respective temperature factors refined to anomalously low values.

Electron density for the NADH is displayed in Figure 5a, and a close-up view of the active site for the reduced enzyme is shown in Figure 6. As can be seen from the electron density, the nicotinamide ring adopts the *anti* conformation in relationship to the ribose as observed in the original structure of the enzyme solved in the presence of UDP-phenol (Bauer *et al.*, 1991). As expected, the nicotinamide ring is not planar but slightly puckered. In addition, the carboxamide group is tilted away from the approximate plane of the nicotinamide ring by  $63^\circ$ . Both riboses in the NADH

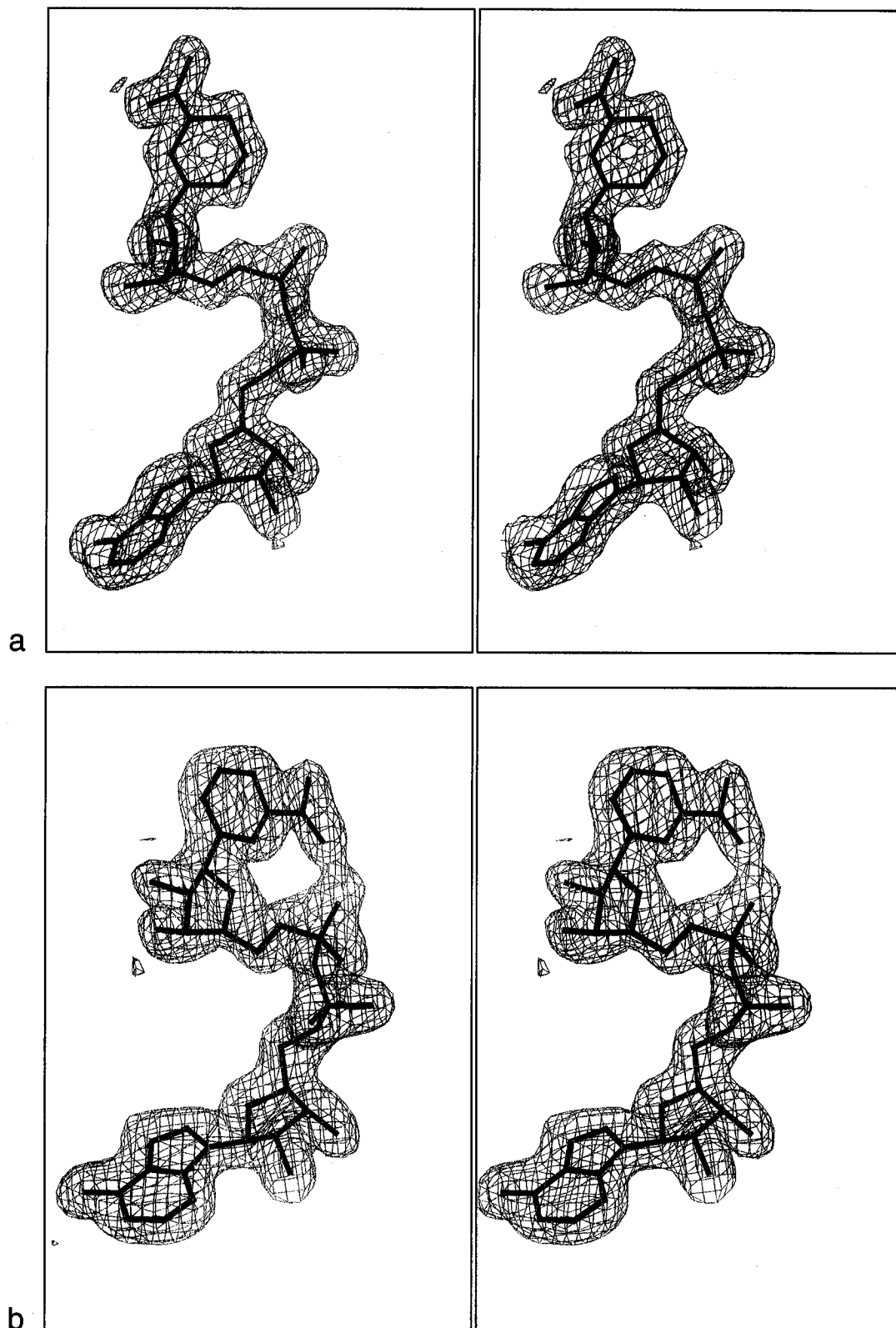


FIGURE 5: Observed electron densities corresponding to the dinucleotide cofactors. The electron density maps shown correspond to (a) the reduced and (b) the oxidized forms of the cofactor calculated to 1.8- and 2.0-Å resolution, respectively. Coefficients employed for the map calculations were of the form  $(2F_o - F_c)$ , where  $F_o$  was the native structure factor amplitude and  $F_c$  was the calculated structure factor amplitude.

cofactor adopt the  $C_2'$ -endo conformation. The binding pocket for NADH is formed by amino residues residing in the N-terminal domain with a total of 34 contacts equal to or below 3.2 Å between the protein and the dinucleotide. Potential hydrogen bonds between the protein and the dinucleotide are shown schematically in Figure 7a. There

are six water molecules important in the binding of the dinucleotide to the enzyme with two hydrogen bonding to the phosphoryl oxygens, two associated with the nicotinamide ribose, one interacting with the carboxamide group, and one situated near the adenine ring. The carboxamide group of the NADH is further anchored to the protein such

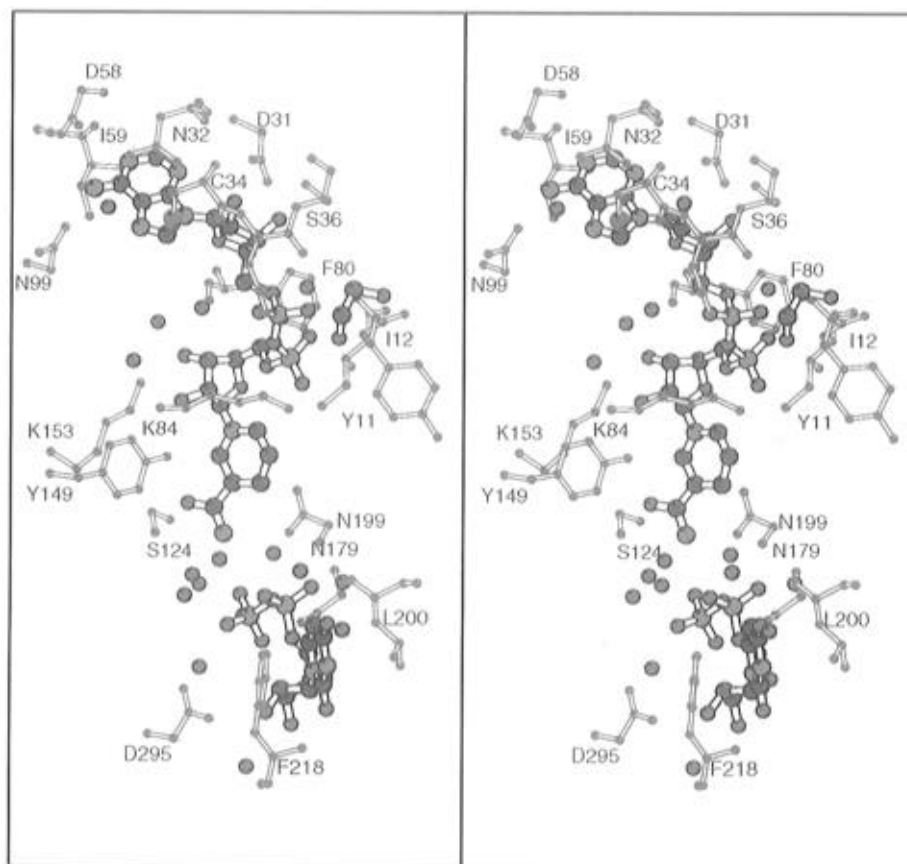


FIGURE 6: Close-up view of the active site of the epimerase/UDP/NADH complex. Only those amino acid residues located within approximately 3.2 Å of the nucleotides are displayed. Ordered water molecules are displayed as red spheres. For the sake of clarity near the UDP molecule, Phe 178, Ala 216, Arg 231, and Arg 292 were omitted from the drawing. Their roles in nucleotide binding are indicated in Figure 7b.

that its oxygen and nitrogen atoms lie within 2.4 Å of O' of Ser 124 and 3.2 Å of the carbonyl oxygen of Phe 178, respectively. Tyr 149 serves as a bridge to the oxygen of the carboxamide moiety (2.7 Å) and the 2'-hydroxyl group of the nicotinamide ribose (2.8 Å). The  $\epsilon$ -nitrogen of Lys 153 is situated at 2.8 Å from the 3'-hydroxyl group of the nicotinamide ribose. Those amino acid residues in contact with the phosphoryl oxygens include Tyr 11 and Ile 12 through their backbone amide hydrogens and Lys 84 and Asn 35 through their side-chain functional groups. One of the phosphoryl oxygens lies within 3.0 Å to a hydroxyl group contributed by the bound ethylene glycol. The adenine ribose of the dinucleotide interacts with the hydroxyl group of Ser 36, the carboxylate group of Asp 31, and the backbone amide hydrogen of Asn 35 as indicated in Figure 7a. There are four potential interactions between the protein and the adenine ring of the dinucleotide. In addition, a water molecule lies within 3.1 Å of N7 of the base.

Potential hydrogen bonds between the protein and UDP are indicated schematically in Figure 7b. As can be seen, the interactions are quite extensive with the binding pocket for UDP formed by amino acid residues from the C-terminal domain. There are 22 contacts equal to or below 3.2 Å between UDP and the protein. As in the NADH, the ribose adopts the  $C_2'$ -endo conformation. Ten water molecules participate in anchoring the nucleotide to the protein, seven of which are hydrogen bonded to the phosphoryl oxygens. The carbonyl oxygen at C4 of the uridine ring interacts with two of these water molecules, and the tenth water molecule is hydrogen bonded to the 3'-hydroxyl group of the ribose.

In addition to the two waters, the uridine moiety is positioned within hydrogen-binding distance to the backbone atoms contributed by Ala 216 and Phe 218 as indicated in Figure 7b. Finally, the 2'-hydroxyl group of the ribose interacts with the carboxylate group of Asp 295.

**Description of the Epimerase/UDP/NAD<sup>+</sup> Complex.** The overall secondary and tertiary structure of the oxidized form of epimerase is essentially identical to that described above for the reduced form. Of the 358 water molecules positioned into the electron density map, 80 have temperature factors below 30.0 Å<sup>2</sup>. As in the reduced enzyme structure, two sodium ions, one ethylene glycol molecule, and one di(ethylene glycol) have been modeled into the electron density. Electron density for the oxidized dinucleotide is displayed in Figure 5b, and a stereo representation of the active site may be found in Figure 8. Schematic representations of the protein/nucleotide interactions are shown in Figure 9. All the ribose moieties adopt the  $C_2'$ -endo conformation. There are 35 protein/dinucleotide contacts equal to or below 3.2 Å. The hydrogen-bonding patterns about the adenine ribose portion of the oxidized dinucleotide are virtually identical, within experimental error, to those observed in the reduced enzyme. One of the most striking differences, however, between the reduced and oxidized forms of epimerase is the relationship of the nicotinamide ring to the ribose. In the oxidized form, the nicotinamide ring is in the *syn* rather than *anti* conformation. In addition, the carboxamide group lies in the plane of the nicotinamide ring. Due to the movement of the nicotinamide ring by a rotation of approximately 180° about the glycosidic bond,

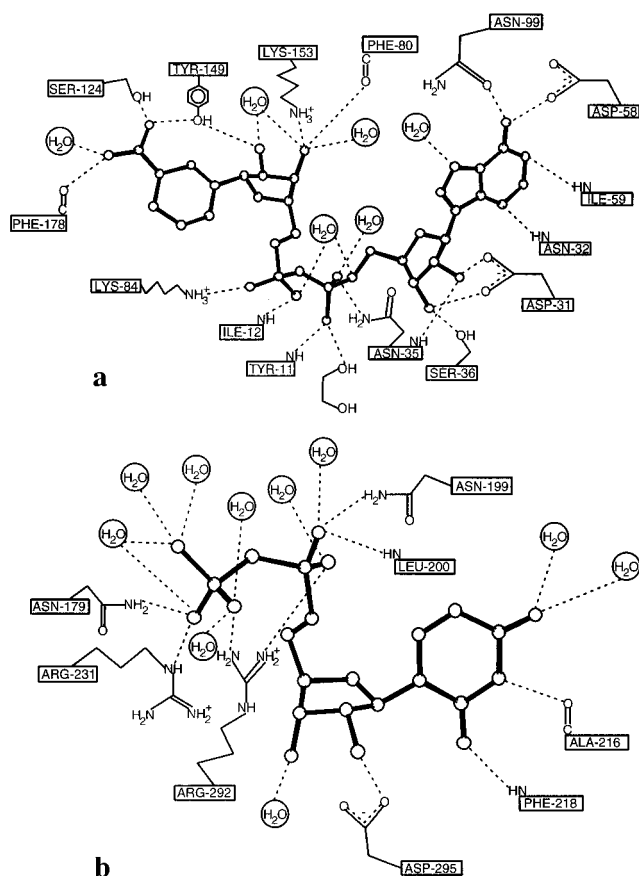


FIGURE 7: Schematic representation of the hydrogen-bonding patterns observed between the reduced protein and the nucleotides. Possible interactions between epimerase and the NADH and UDP moieties within 3.2 Å are shown in (a) and (b), respectively.

several protein/cofactor interactions in this region have changed significantly. Most notable of these changes include the interaction of Lys 84 with both a phosphoryl oxygen and the nitrogen of the carboxamide group, the loss of Ser 124 and Phe 178 in the hydrogen-bonding motif, and the addition of Tyr 177 to the binding pocket. The nitrogen of the carboxamide group also lies within 2.3 Å to one of the phosphoryl oxygens of the dinucleotide.

Quite strikingly, the interactions between the oxidized enzyme and UDP are less extensive than those observed in the reduced protein model. There are only 16 contacts equal to or below 3.2 Å. Four water molecules are directly involved in UDP binding as opposed to ten in the reduced enzyme, and there is only one potential interaction at 2.9 Å between N3 of the uridine ring and the carbonyl oxygen of Ala 216. There are no obvious electrostatic interactions between the protein and the ribose of the uridine nucleotide. Unlike that observed in the reduced structure, Asn 199, Phe 218, Arg 231, and Asp 295 do not play significant roles in nucleotide binding. These striking differences in UDP binding between the oxidized and reduced forms of the protein most likely explain the observation that uridine nucleotides bind 100–1000-fold more tightly to epimerase/NADH than to epimerase/NAD<sup>+</sup> (Wong & Frey, 1977).

**Comparison of the Oxidized and Reduced Forms of the Enzyme.** The  $\alpha$ -carbon positions for the two forms of epimerase superimpose with a root-mean-square deviation of 0.36 Å. Slight differences between the two proteins are confined to five regions delineated by Ser 122 to Asn 131, Arg 176 to Gly 182, Pro 193 to Tyr 233, His 287 to Ala

301, and Gln 329 to Gln 334. These regions are shown in Figure 10. In the absence of these residues, the  $\alpha$ -carbons for the oxidized and reduced enzymes superimpose with a root-mean-square deviation of 0.21 Å. The most notable changes in structure between the two forms of epimerase occur at Phe 178 and Phe 218 as displayed in Figure 10. In the reduced form, Phe 178 faces away from the nicotinamide ring of the dinucleotide whereas in the oxidized protein, this residue moves in toward the binding pocket. Phe 218 forms a parallel stacking interaction with the uridine ring of the mononucleotide in the reduced enzyme. This interaction is disrupted in the enzyme/NAD<sup>+</sup> structure as can be seen in Figure 10. In the oxidized but not the reduced protein, multiple conformations are observed in the electron density map for both Phe 178 and Phe 218. One of the conformations is shown in black in Figure 10. The second conformation is identical to that observed in the reduced protein and is depicted in red in the figure. Note that the enzyme employed for the crystallization experiments was not fully oxidized and these multiple conformations most likely arise from that fact. In a fully oxidized protein, Phe 178 and Phe 218 probably adopt the conformations as outlined in black in Figure 10.

With respect to solvent, there are 115 water molecules that superimpose within approximately 0.4 Å between the oxidized and reduced forms of epimerase. Many of these waters are located in nearly identical positions within the nucleotide binding pockets. One striking difference between the two forms of the protein occurs in the region surrounding Ser 124. In the reduced enzyme, O' of Ser 124 lies within 3.0 Å of the backbone amide nitrogen of Thr 126 and 2.9 Å of its side-chain hydroxyl group. In addition, there is a very close approach of 2.4 Å between O' of Ser 124 and the nitrogen of the carboxamide group of NADH. In the oxidized enzyme, O' of Ser 124 forms hydrogen bonds with Thr 126 in a similar manner, but rather than the third hydrogen bond occurring between its side chain and the carboxamide group of the dinucleotide, a solvent molecule moves into the binding pocket and replaces this interaction.

In the original model of epimerase complexed with the substrate analog, UDP-phenol, the NAD<sup>+</sup> adopted the *anti* rather than *syn* conformation although the enzyme employed for crystallization experiments was of the oxidized form (Bauer *et al.*, 1992). This was somewhat surprising since epimerase transfers a hydride to the B-side of the nicotinamide ring, and as such it was anticipated that the dinucleotide would adopt the conformation observed in B-side specific dehydrogenases, namely the *syn* arrangement (Wu & Houk, 1991). The current studies demonstrate that, in the absence of a benzene moiety, the position of the nicotinamide ring, in relationship to the ribose, depends upon the oxidation state of the cofactor. Furthermore, the high-resolution models described here do not implicate a "traditional" base, such as an aspartate, glutamate, or histidine, within 5 Å of the active site. As such, the identity of the putative active site base is still open to question.

**Basis for the Strong Binding of NAD<sup>+</sup> to Epimerase.** In decided contrast to the NAD<sup>+</sup>-dependent dehydrogenases where the binding of the dinucleotide is readily reversible, epimerase binds the cofactor in such a manner that its removal results in irreversible denaturation of the enzyme (Frey, unpublished results). The current structural model for epimerase/NAD<sup>+</sup> shows a total of 35 protein–dinucleotide

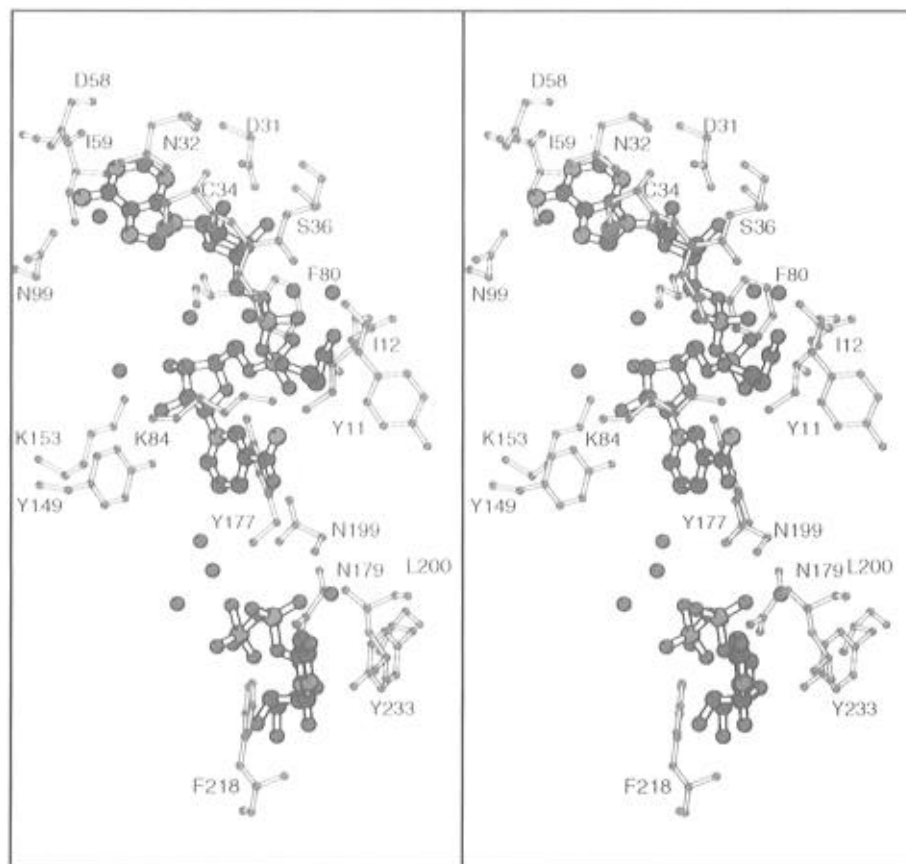


FIGURE 8: Close-up view of the active site of the epimerase/UDP/NAD<sup>+</sup> complex. Only those amino acid residues located within approximately 3.2 Å of the nucleotides are displayed. As in Figure 6, Ala 216, Arg 231, and Arg 292 were omitted from the drawing.

contacts equal to or below 3.2 Å, 7 of which are contributed by ordered water molecules. By comparison with the X-ray coordinates refined to 1.8-Å resolution and obtained from the Brookhaven Protein Data Bank, malate dehydrogenase (1BDM), horse liver alcohol dehydrogenase (2OHX), and glyceraldehyde-3-phosphate dehydrogenase (1GD1) demonstrate 22, 25, and 27 contacts, respectively. In glyceraldehyde-3-phosphate dehydrogenase, 15 of these contacts are contributed by solvent molecules including one sulfate ion. The greater number of enzyme/NAD<sup>+</sup> interactions in epimerase extends to all parts of the dinucleotide, but the effect is especially striking near the adenosyl portion. The adenine ring in epimerase is locked into place by five hydrogen bonds, four contributed by protein side chains and one by a water molecule. In the case of the above-mentioned dehydrogenases, however, the adenine rings demonstrate few specific interactions with the proteins. Specifically, in both malate dehydrogenase and alcohol dehydrogenase, there is only one water molecule located within 3 Å of the adenosyl groups. In glyceraldehyde-3-phosphate dehydrogenase, the guanidinium group of Arg 77 and an ordered water molecule form the only specific hydrogen-bonding interactions with the adenine group.

In summary, the high-resolution structural studies presented here demonstrate that the conformation of the nicotinamide ring of the NAD<sup>+</sup>/NADH cofactor, when bound to epimerase, is dependent upon its oxidation state. Two distinct hydrogen-bonding patterns are available on the protein to accommodate such differences. The tight binding of the dinucleotide to epimerase, in contrast to the NAD<sup>+</sup>-dependent dehydrogenase, is due to the more extensive

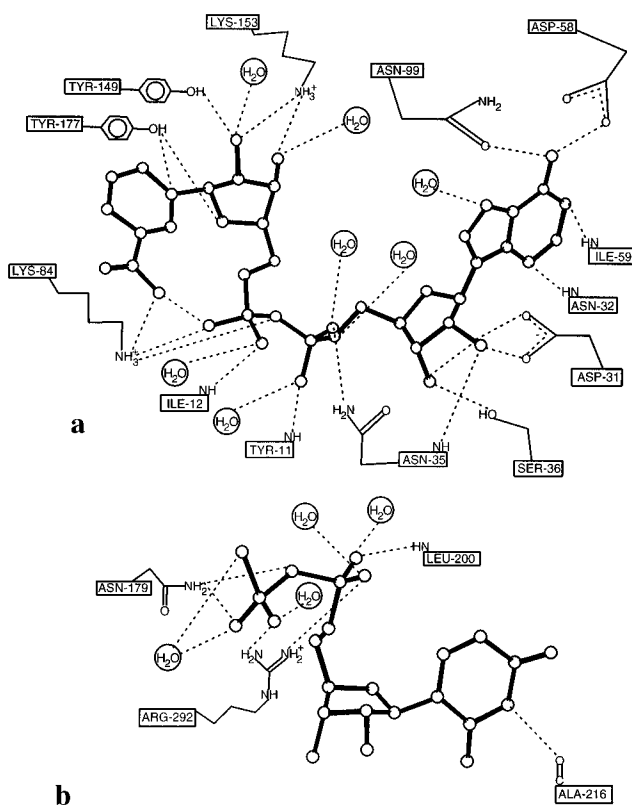


FIGURE 9: Schematic representation of the hydrogen-bonding patterns observed between the oxidized protein and the nucleotides. Possible interactions between epimerase and the NAD<sup>+</sup> and UDP moieties within 3.2 Å are shown in (a) and (b), respectively.

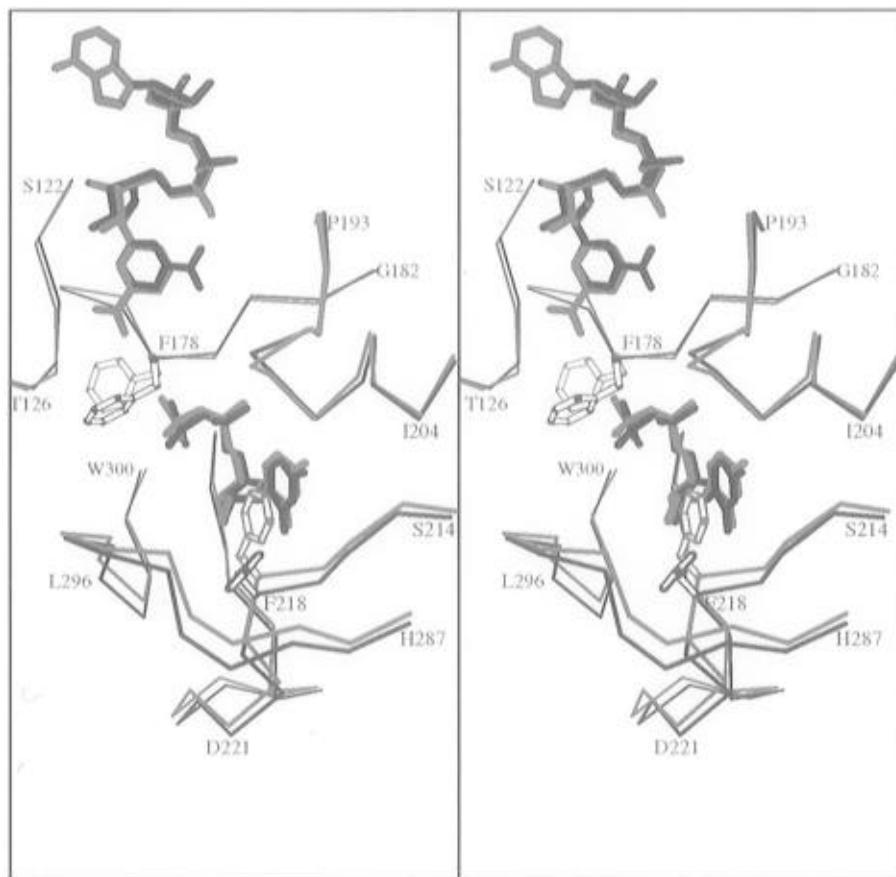


FIGURE 10: Comparison of the  $\alpha$ -carbon positions for the reduced and oxidized forms of epimerase. The reduced and oxidized forms of the enzyme are shown in red and black, respectively. Only those regions that differ significantly between the two protein forms are included. Phe 178, Phe 218, and the nucleotides are also shown.

interactions between the cofactor and the protein. Likewise, the higher binding affinity of the reduced epimerase for UDP is due to more extensive protein/mononucleotide interactions. Perhaps most intriguing in these current epimerase models is the apparent absence of a general base within the active site region. Experiments designed to study the three-dimensional structure of the NADH/UDP-glucose abortive complex are in progress with the goal of addressing this issue.

## ACKNOWLEDGMENT

We thank Dr. W. W. Cleland for helpful discussions and advice.

## REFERENCES

- Bauer, A. J., Rayment, I., Frey, P. A., & Holden, H. M. (1991) *Proteins: Struct., Funct., Genet.* 9, 135–142.
- Bauer, A. J., Rayment, I., Frey, P. A., & Holden, H. M. (1992) *Proteins: Struct., Funct., Genet.* 12, 372–381.
- Bertland, A. U., & Kalckar, H. M. (1968) *Proc. Natl. Acad. Sci. U.S.A.* 61, 629–635.
- Frey, P. A. (1987) in *Pyridine Nucleotide Coenzymes: Chemical, Biochemical, and Medical Aspects* (Dolphin, D., Poulson, R., & Avramovic, O., Eds.) pp 461–511, John Wiley & Sons, Inc., New York.
- Fox, G. C., & Holmes, K. C. (1966) *Acta Crystallogr.* 20, 886–891.
- Glasfeld, A., Zbinden, P., Dobler, M., Benner, S. A., & Dunitz, J. D. (1988) *J. Am. Chem. Soc.* 110, 5152–5157.
- Jones, A. T. (1985) *Methods Enzymol.* 115, 157–171.
- Kabsch, W. (1988a) *J. Appl. Crystallogr.* 21, 67–71.
- Kabsch, W. (1988b) *J. Appl. Crystallogr.* 21, 916–924.
- Kang, U. G., Nolan, L. D., & Frey, P. A. (1975) *J. Biol. Chem.* 250, 7099–7105.
- Kraulis, P. J. (1991) *J. Appl. Crystallogr.* 24, 946–950.
- Lemaire, H.-G., & Müller-Hill, B. (1986) *Nucleic Acids Res.* 14, 7705–7711.
- Navaza, J. (1987) *Acta Crystallogr.* A43, 645–653.
- Reddy, B. S., Saenger, W., Mühlegger, K., & Weimann, G. (1981) *J. Am. Chem. Soc.* 103, 907–914.
- Rossmann, M. G. (1972) *The Molecular Replacement Method. A Collection of Papers on the Use of Non-Crystallographic Symmetry*, Gordon and Breach, New York.
- Swanson, B. A., & Frey, P. A. (1993) *Biochemistry* 32, 13231–13236.
- Tronrud, D. E., Ten Eyck, L. F., & Mathews, B. W. (1987) *Acta Crystallogr.* A43, 489–501.
- Vanhooke, J. L., & Frey, P. A. (1994) *J. Biol. Chem.* 269, 31496–31504.
- Viswamitra, M. A., Post, M. L., & Kennard, O. (1979) *Acta Crystallogr.* B35, 1089–1094.
- Walsh, C. (1979) *Enzymatic Reaction Mechanisms*, Freeman, San Francisco.
- Wilson, D. B., & Hogness, D. S. (1964) *J. Biol. Chem.* 239, 2469–2481.
- Wilson, D. B., & Hogness, D. S. (1969) *J. Biol. Chem.* 244, 2132–2136.
- Wong, S. S., & Frey, P. A. (1977) *Biochemistry* 16, 298–305.
- Wong, S. S., Cassim, J. Y., & Frey, P. A. (1978) *Biochemistry* 17, 516–520.
- Wu, Y. D., & Houk, K. N. (1991) *J. Am. Chem. Soc.* 113, 2353–2358.

BI952715Y